Magnetically-Controlled Logic Gates of Graphene Plasmons Based on Non-Reciprocal Coupling

Bofeng Zhu, Guobin Ren, Yixiao Gao, Beilei Wu, Chenglong Wan, and Shuisheng Jian

***Abstract*—In this paper, we propose magnetically-controlled logic gates of graphene plasmons based on non-reciprocal coupling within the multilayer graphene waveguide structure. The magnetooptical effect of semiconductor substrate leads to the difference in modal indices of graphene plasmons in opposite directions and non-reciprocal coupling, which is investigated by both coupled mode theory (CMT) and finite elements methods (FEM). Such a mechanism enables the design of magnetically- controlled NOT logic gate, whose output logic can be inversed by reversing the plasmons propagation directions. Furthermore, according to the Boolean algebra, we design two functional logic gates performing as OR (AND) logic gates for one direction of input plasmons, while NAND (NOR) logic gates for the reversed input direction. Minimum extinction ratios as 13.6 or 17.5 dB can be obtained for OR (NAND) or AND (NOR) logic gate. The proposed magnetically-controlled logic gates may provide new inspiration to non-reciprocal graphene plasmons devices.**

***Index Terms*—Graphene plasmons, logic gates, magneto-optical effect, non-reciprocal coupling.**

I. Introduction

SURFACE plasmons (SPs) are electromagnetic excitations propagating along the interface between dielectrics and conductors [1]. Graphene is a semiconductor with a two-dimensional honeycomb form of arranged carbon atoms in a lattice [2], possessing an extremely high quantum efficiency for light–matter interactions and contains plasmons (graphene plasmons (GPs)) with unusual properties [3]. To date, several works have been involved in the investigations of coupling in multilayer graphene waveguide system [4]–[6]. Routing of GPs within the multilayer graphene waveguide structure has been investigated [4], [5] and revolutions of supported modes have been analyzed [6].

Nanoscale all-optical logic gate devices have attracted enormous attention because of their remarkable properties compared with traditional electronic logic gates [7] and therefore are capable for applications in fields such as optical computing and ultrahigh speed information processing [8]. Previously, magnetic-controlled semiconductor logic gates have been proposed [9], in which the logic functions are realized by controlling the generation and recombination of carriers in a semiconductor p-n bilayer channel. Meanwhile, electronically biased GPs logic gates have been proposed [10] and shown superior performances to traditional optical logic gates. However, in such architecture, graphene layers are individually biased and each kind of functional logic gate needs specific bias voltages, which may introduce implementation complexities. Recently, directionally exciting of GPs on the magneto-optical substrate has been investigated [11]. The magneto-optical effect based unsymmetrical dispersion relation provides a potential route to control GPs via applied magnetic field.

In this paper we propose magnetically-controlled GPs logic gates based on non-reciprocal coupling. In Section II, the coupled mode theory (CMT) has been adopted and numerically verified to describe the non-reciprocal coupling, revealing its functionality as a logic gate controlled by the applied magnetic field and plasmons propagation directions. In Sections III and IV, we respectively design two magnetically-controlled logic gates (i.e., OR or AND) based on the Boolean algebra and reveal their functionalities as NAND or NOR logic gates for the reversed plasmons propagation direction. Afterwards the corresponding truth tables and field profiles are presented. Finally we draw conclusions.

II. Theoretical Descriptions of Non-Reciprocal Coupling

We first analyze the non-reciprocal coupling within multilayer graphene waveguide structure. In the mid-infrared frequency range, the conductivity of graphene can be modeled with a semi-classical Drude model including the temperature correction ($T = 300$ K) [1] and should not be affected by the magnetic field oriented parallel to the graphene sheet [2]. The carrier relaxation time τ is set as $\tau = 0.45$ ps, the carrier mobility is $u = 10^4$ cm^2/(V·s) and the Fermi velocity is $v_f = 10^6$ m/s [3]. By treating the graphene as an ultrathin layer with thickness $d = 0.34$ nm, the tangential permittivity of graphene can be expressed as $\varepsilon_{g,t} = 2.5 - i\sigma/\omega\varepsilon_0 d$ [3]. The surface-normal permittivity of graphene is assumed as $\varepsilon_{g,n} = 2.5$, based on the dielectric constant of graphite [1], [4]. The chemical potential of graphene is set as $\mu_c = 0.45$ eV, which can be implemented through chemical doping [5]. For the magnetic-optical material, the dielectric permittivity tensor with magnetic field B can be expressed as [2], [6]

$$\overleftrightarrow{\varepsilon}_s \approx \varepsilon_\infty \begin{bmatrix} \varepsilon_{xx} & i\varepsilon_{xy} & 0 \\ -i\varepsilon_{xy} & \varepsilon_{yy} & 0 \\ 0 & 0 & \varepsilon_{zz} \end{bmatrix}, \quad (1)$$

Manuscript received April 13, 2015; revised August 15, 2015 and October 8, 2015; accepted October 13, 2015. This work was supported by the National Natural Science Foundation of China under Grants 61178008 and 61275092.

B. Zhu, G. Ren, Y. Gao, B. Wu, and S. Jian are with the Key Laboratory of All Optical Network and Advanced Telecommunication Network of EMC, Beijing Jiaotong University, Beijing 100044, China (e-mail: 12111033@bjtu.edu.cn; gbren@bjtu.edu.cn; yixiao68@gmail.com; 12111034@bjtu.edu.cn; ssjian@bjtu.edu.cn).

C. Wan is with the Department of Electrical and Electronic Engineering, University of Bristol, Bristol BS8 1TH, U.K. (e-mail: cw7679@bristol.ac.uk).

Color versions of one or more of the figures in this paper are available online at http://ieeexplore.ieee.org.

Digital Object Identifier 10.1109/JSTQE.2015.2493958

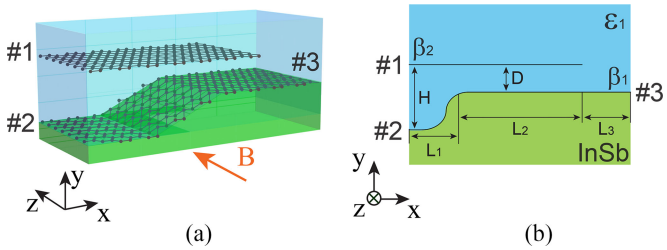

Fig. 1. Schematic view (a) and the cross section on plane xy (b) of the NOT logic gate, the applied magnetic field (red arrow) is parallel to z-axis.

where $\varepsilon_\infty = 15.68$ is the high-frequency permittivity. The tensor elements are $\varepsilon_{xx} = \varepsilon_{yy} = 1 - \omega_p^2/(\omega^2 - \omega_c^2), \varepsilon_{xy} = \omega_c\omega_p^2/\omega(\omega^2 - \omega_c^2), \varepsilon_{zz} = 1 - \omega_p^2/\omega^2$ with angular frequency ω. The $\omega_p = [Ne^2/(\varepsilon_\infty\varepsilon_0 m^*)]^{1/2}$ and $\omega_c = eB/m^*$ are the plasma frequency and the cyclotron frequency composed of the electron density $N = 2 \times 10^{24}$ m^{-3} by moderate doping [7], effective mass $m^* = 0.014m_e$, electric charge e and electron rest mass m_e.

Sketched in Fig. 1(a) and (b) are the schematic and cross section of coupled graphene layers system, which is composed of two vertically placed graphene layers. The top graphene layer is embedded in the dielectric medium with permittivity $\varepsilon_1 = 1.4$ and bottom graphene layer is placed on a doped InSb substrate with an applied magnetic field B along z direction. We assume the GPs are input from port #1 and output from port #2 or port #3. Through our discussion, the parameters are fixed at $L_1 = 135$ nm, $L_3 = 100$ nm and $H = 175$ nm. The overlap length L_2 and interspace length D are variables. The GPs propagation constant β_1 on bottom layer can be obtained by numerically solving dispersion relation as [2],

$$\begin{aligned} &\frac{\varepsilon_1}{k_2} + \frac{\varepsilon_{xx}^2 - \varepsilon_{xy}^2}{k_1\varepsilon_{xx} + \beta_1\varepsilon_{xy}} + \frac{i\sigma}{\omega\varepsilon_0} = 0, \\ &k_1 = \sqrt{\beta_1^2 - \left[\omega^2(\varepsilon_{xx}^2 - \varepsilon_{xy}^2)/\varepsilon_{xx}\right]/c^2}, \\ &k_2 = \sqrt{\beta_1^2 - (\varepsilon_1\omega^2/c^2)}. \end{aligned} \tag{2}$$

For the uncoupled top layer graphene, the dispersion relation of GPs can be expressed as [3],

$$\beta_2 \approx \frac{2\pi\hbar^2\varepsilon_0\varepsilon_1}{e^2\mu_c}\left(1 + \frac{i}{\omega\tau}\right)\omega^2, \tag{3}$$

in which the dispersion and loss of dielectric are neglected and ε_0 is the permittivity of free space. Based on Eqs. (2) and (3), the real modal indices of GPs on top and bottom layers along x^+ direction with respect to the free space wavelength and medium permittivity ε_1 under moderate magnetic field $B = \pm 3$ T [8] or no magnetic bias are presented in Fig. 2(a) and (c), respectively. Accordingly, the propagation length of GPs for such situations are shown in Fig. 2(b) and (d), in which the propagation length is defined as $L_p = 1/[2\mathrm{Im}(\beta)]$ with β is the propagation constant of plasmons [9].

As shown in Fig. 2, as the wavelength increases or the permittivity ε_1 decreases, the real modal index decreases while

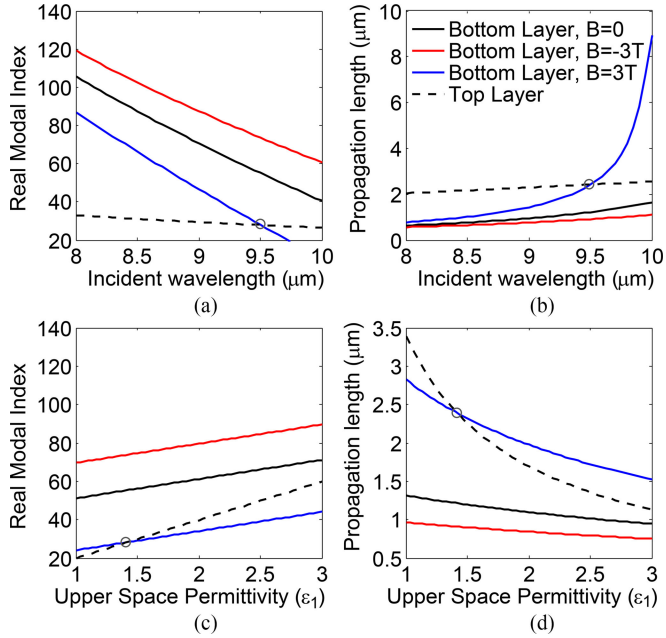

Fig. 2. Dependencies of the real modal index and propagation length of GPs along x^+ direction on the wavelengths (a), (b) and upper space medium permittivity ε_1 (c), (d) for opposite magnetic fields. The upper space permittivity is $\varepsilon_1 = 1.4$ in (a) and (b) while the wavelength is $\lambda = 9.5$ μm in (c) and (d).

the propagation length L_p increases, since higher modal index generally means the higher modal confinement and therefore the larger modal attenuation. Compared with the modal indices of plasmons on bottom layer under $B = 0$, the plasmons along x^+ direction under $B = -3$T ($B = 3$T) owe higher (lower) modal indices and simultaneously shorter (longer) propagation lengths. At the wavelength $\lambda = 10$ μm and $\varepsilon_1 = 1.4$, the propagation length can be near $L_p = 9$ μm. It is worth noting that, at $\lambda = 9.5$ μm, the GPs supported on top layer possess nearly the same real modal index or propagation length as the plasmons on bottom layer under $B = 3$T while obvious differences appear between those and the ones under $B = -3$T. More importantly, we could obtain the same real modal index of GPs on bottom layer via simultaneously reversing the direction of magnetic field B and the direction of plasmons propagation [2], which means the plasmons along x^+ direction with $B = -3$T (solid red lines) possess the same real indices as those along x^- direction with $B = 3$T. Such conclusion can be attributed to the non-square propagation constant in the second term of dispersion relation in Eq. (2) and potentially provides a route to achieve non-reciprocal coupling between two graphene layers.

To achieve complete energy transfer in the multilayer graphene waveguides structure, it is essential to ensure the modal wavenumber matching of plasmons on two graphene layers [10], otherwise the energy coupling is weakened once the two wavenumbers differ greatly. Therefore, if we choose wavelength $\lambda = 9.5$ μm, complete coupling of GPs between the two layers emerges along x^+ direction under $B = 3$T while in contrast weak coupling appears under $B = -3$T or when GPs are input from port #3 (with $B = 3$T). For such a coupling system, the transmittances from top graphene layer to the bottom layer can be calculated through CMT. For both layers, the plasmons

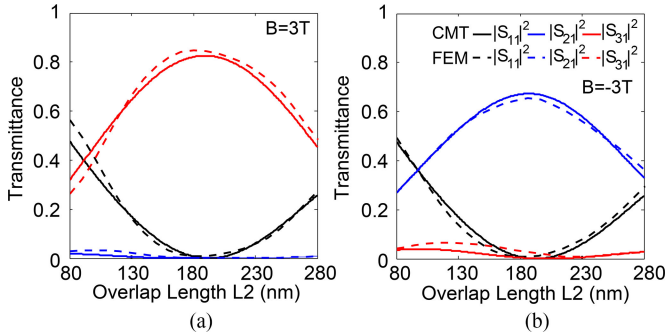

Fig. 3. The transmittances $|S_{21}|^2$, $|S_{31}|^2$ and reflectance $|S_{11}|^2$ with respect to overlap length L_2 for opposite magnetic fields. (a) for $B = 3$ T and (b) for $B = -3$T. The wavelength $\lambda = 9.5$ μm and $D = 40$ nm.

amplitudes at $x = L_1$ and $x = L_1 + L_2$ satisfy the relation as [10],

$$\begin{bmatrix} a_1(L_1+L_2) \\ a_2(L_1+L_2) \end{bmatrix} = \begin{bmatrix} A & B \\ C & D \end{bmatrix} \begin{bmatrix} a_1(L_1) \\ a_2(L_1) \end{bmatrix}, \tag{4}$$

in which a_1 and a_2 represent the wave amplitudes in bottom and top layers, respectively. And accordingly, the transmittances within the overlap region L_2 can be expressed as,

$$\begin{aligned} |a_1(L_1+L_2)/a_1(L_1)|^2 &= |A|^2, \\ |a_2(L_1+L_2)/a_1(L_1)|^2 &= |C|^2, \end{aligned} \tag{5}$$

in which the elements A and C are defined by,

$$\begin{aligned} A &= \cos(\beta_0 L_2) + i\left[(\beta_2-\beta_1)/(2\beta_0)\right] sin(\beta_0 L_2), \\ C &= (\kappa_{21}/\beta_0) sin(\beta_0 L_2), \\ \beta_0 &= \sqrt{\left[(\beta_1-\beta_2)/2\right]^2 + |\kappa_{12}|^2}, \\ |\kappa_{12}| &= (1/2)\sqrt{(\beta_d-\beta_c)^2 - (\beta_1-\beta_2)^2}. \end{aligned} \tag{6}$$

The $\kappa_{12=}\kappa_{21}^*$ is the coupling constant between top and bottom layers. The propagation constant β_d or β_c denotes the differential or common mode in the double graphene layer waveguide structure [10, 11], which can be derived by numerical or analytical methods. Finally the transmittances can be obtained by combining Eq. (5) and modal attenuation on top and bottom layers with the coupling loss is neglected here. To verify the accuracy of CMT model, we conduct both analytical and numerical investigations on transmittances or reflectance with respect to the overlap length L_2 under opposite magnetic fields in Fig. 3(a) and (b). The wavelength is $\lambda = 9.5$ μm and $D =$ 40 nm. All the numerical solutions have been performed by the software package (COMSOL) based on the finite elements methods (FEM).

In Fig. 3(a) and (b), good consistency can be observed between the theoretical results based on CMT and numerical results based on FEM. For applied magnetic field $B = 3$T, complete energy transferring emerges between ports #1 and #3. In contrast, complete energy transferring exists between ports #1 and #2 for magnetic field $B = -3$T. Such phenomenon can be attributed to the different coupling mechanisms under opposite magnetic fields. For input plasmons along x^+ direction and

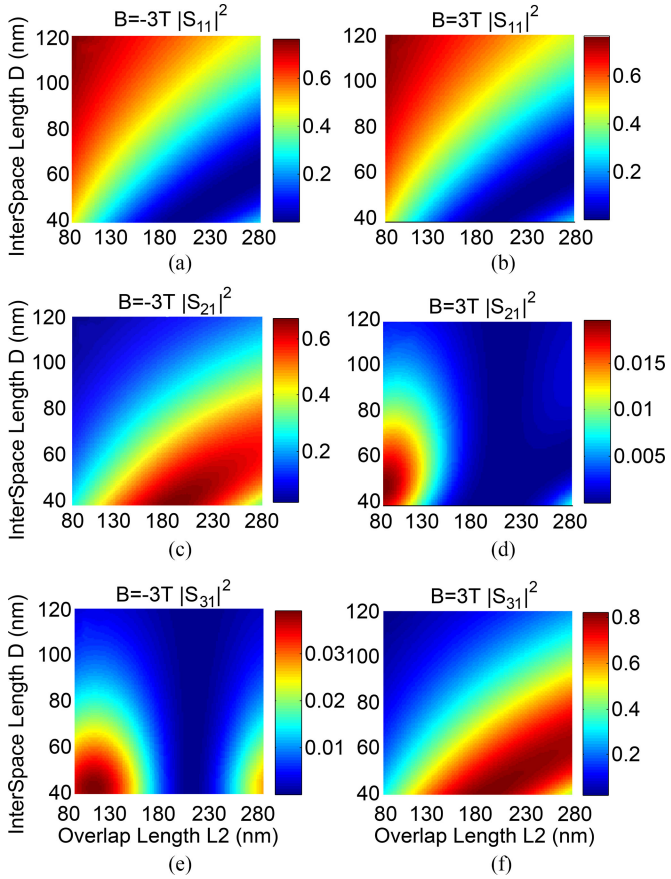

Fig. 4. The contour diagrams of the reflectance and transmittances ($|S_{11}|^2$, $|S_{21}|^2$ and $|S_{31}|^2$) with respect to the interspace length D and overlap length L_2. Figures (a), (c), (e) are for magnetic field $B = -3$T while figures (b), (d), (f) are for magnetic field $B = 3$T. The wavelength is $\lambda = 9.5$ μm.

magnetic field $B = 3$T, complete energy transferring occurs within overlap region L_2 before the GPs reaching the right end point of top graphene layer. The uncoupled energy is reflected at the end point and output from port #1. Few energy would be coupled to port #2 due to the great modal wavenumber mismatch between plasmons on top and bottom layers along x^- direction. While for the input plasmons under magnetic field B = –3T, the situation is reversed. Weak coupling appears first for plasmons within region L_2 before reaching the terminal point. Afterwards complete energy transferring occurs when GPs are reflected back, the uncoupled energy outputs from port #1. In the two cases of Fig. 3, although all of the plasmons energy on the top graphene waveguide is coupled to the bottom graphene waveguide, the maximum transmittance is smaller than one due to the plasmons modal attenuation. Moreover, since simultaneously reversing magnetic field direction and plasmons propagation direction lead to the same real modal index [2], we can conclude that transmittance from port #1 to port #3 (i.e., $|S_{31}|^2$ with $B = 3$T) in Fig. 3(a) is similar to the one from port #3 to port #1 (i.e., $|S_{13}|^2$ with $B = -3$T).

As shown in Fig. 3, the CMT model can well explain the non-reciprocal coupling. For better presentation, we have calculated the reflectance and transmittances ($|S_{11}|^2$, $|S_{21}|^2$, and $|S_{31}|^2$) under opposite direction of magnetic fields. The results are shown in Fig. 4, in which the Fig. 4(a), (c), (e) are for

magnetic field B = –3T while the Figs. 4(b), (d), (f) are for magnetic field B = 3 T. As shown in Fig. 4(a) and (b), most of the input energy is reflected back at short overlap length L_2 and large interspace length D. The reason is that the complete energy transfer condition is not satisfied and plasmons cannot be coupled to the bottom graphene layer, only being reflected at the terminal of top layer and then propagate back to port #1.

As for the Fig. 4(c)–(f), it can be found that the contour diagram of $|S_{21}|^2$ under B = 3T [see Fig. 4(d)] is similar to the contour diagram of $|S_{31}|^2$ under B = –3T [see Fig. 4(e)]. On the other hand, the contour diagram of $|S_{21}|^2$ under B = –3T [see Fig. 4(c)] is similar to the contour diagram of $|S_{31}|^2$ under B = 3T [see Fig. 4(f)]. Such phenomenon illustrates the energy transfer direction in coupling can be tailored by controlling the direction of applied magnetic field. Specifically, in Fig. 4(c) and (f), the overlap length L_2 where strongest coupling occurs increases with the interspace length D, although the direction of energy coupling is from port #1 to port #3 under B = 3T while from port #1 to port #2 under B = –3T. Accordingly, much weaker energy with maximum transmittances below 0.04 outputs from port #2 under B = 3T [see Fig. 4(d)] or port #3 under B = –3T [see Fig. 4(e)]. It is worth noting that there are still differences between Fig. 4(d) and (e) [or between Fig. 4(c) and (f)]. This is because the optical path from port #1 to port #3 is shorter than the one from port #1 to port #2 [see the schematic in Fig. 1(b)], causing more modal attenuation for energy output from port #2.

Here we denote the applied field direction as the input of logic gate (i.e., the field along z^+ direction as logic A = 1 and z^- direction as logic A = 0) and the transmittances through port #3 (in units of dB) as the output of logic gate (i.e., if there is output energy from the port, the output logic is Q = 1). For plasmons input from port #1 and output from port #3, the relation between output logic and input logic can be expressed through Boolean expression as Q = A. In contrast, if the plasmons input from port #3 and the transmittance through port #1 is defined as the output logic, the relation turns into: $Q = \overline{A}$, achieving the function of a NOT logic gate. The non-reciprocal coupling enables us to design a magnetically-controlled logic gate with the output logic can be controlled via reversing magnetic field direction, which is similar to the magnetically-controlled logic gates based on semiconductors [12]. Furthermore, by reversing the plasmons propagation direction, the output logic Q is given by the inversion of input logic A.

III. Magnetically-Controlled OR(NAND) Logic Gates Based on Non-Reciprocal Coupling

In the previous section, we present that the non-reciprocal coupling could find applications in the design of magnetically-controlled logic gates of GPs. Meanwhile, the reverse of plasmons propagation direction leads to the inversion of output logic. In this section, we first design a magnetically-controlled logic gate which behaves as OR logic gate for GPs along x^+ direction while as NAND logic gate for GPs along x^- direction. Sketched in Fig. 5(a) are three graphene layers embedded between doped InSb substrates and one dielectric spacer. The top and bottom InSb substrates are biased with magnetic fields with same amplitude ($|B_1| = |B_2| = 3T$). The magnetic field directions are set as the input logics by denoting the magnetic field B_1 along z^+ direction as input logic A = 1, while the magnetic field B_2 along z^- direction as input logic B = 1 [see Fig. 5(b)]. The GPs either input from port #1 or port #4 with the overlap and interspace lengths are chosen as L_1 = 135 nm, L_2 = 250 nm, L_3 = 150 nm, H = 175 nm and D = 60 nm based on Fig. 4(d), and (f) with wavelength $\lambda = 9.5\ \mu$m.

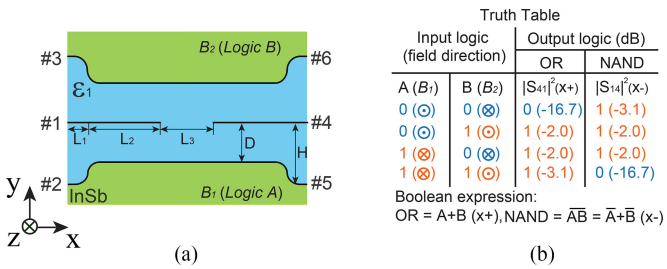

Fig. 5. The schematic of proposed OR (NAND) logic gate. The truth table is shown in (b). The wavelength is $\lambda = 9.5\ \mu$m.

The functionality of such OR(NAND) logic gate is presented through the truth table, which has been shown in the Fig. 5(b). For the left two columns, the values outside the parenthesis indicate the input logics A and B of the device. The markers inside the parenthesis denote the field directions of magnetic field B_1 and B_2 (e.g., for B_1 and B_2 with the directions along z^+ axis, the input logics are A = 1 and B = 0). For the right two columns, the values outside the parenthesis are the output logic of such device. And the transmittances through output ports (in units of dB) under each combination of input logics are shown in the parenthesis (e.g., under input logics A = B = 1 and plasmons input from port #1 along x^+ direction, output logic is Q = 1 with corresponding output energy from port #4 is –3.1 dB).

For the plasmons input from port #1 along x^+ direction, if the strong coupling occurs between input arm and bottom (or top) graphene layers depends on the differences between wave numbers of plasmons on them. Either the magnetic field B_1 along z^+ direction (input logic A = 1) or the magnetic field B_2 along z^- direction (input logic B = 1) ensures the plasmons output from port #4 (output logic Q = 1). Only when B_1 along z^- direction (input logic A = 0) and B_2 along z^+ direction (input logic B = 0) occurs, coupling is suppressed and in such case, the plasmons would be reflected at the right terminal of input arm and coupled to ports #2 and #3 [i.e., output logic Q = 0 in Fig. 6(a)]. The outputs of such an OR logic gate are shown in the truth table of Fig. 5(b), in which the minimum extinction ratios as 13.6 dB can be achieved. Compared with the insertion loss (i.e., 2 dB in truth table) when either of the input logics is high, the loss (i.e., 3.1 dB in truth table) under both high input logics is larger due to the longer optical path and therefore higher modal attenuation. For better presentation, we simultaneously illustrate the normalized electric field profiles according to the four groups of input logics in Fig. 6(a)–(d). The red arrows are power flow directions and white arrows are plasmons input directions.

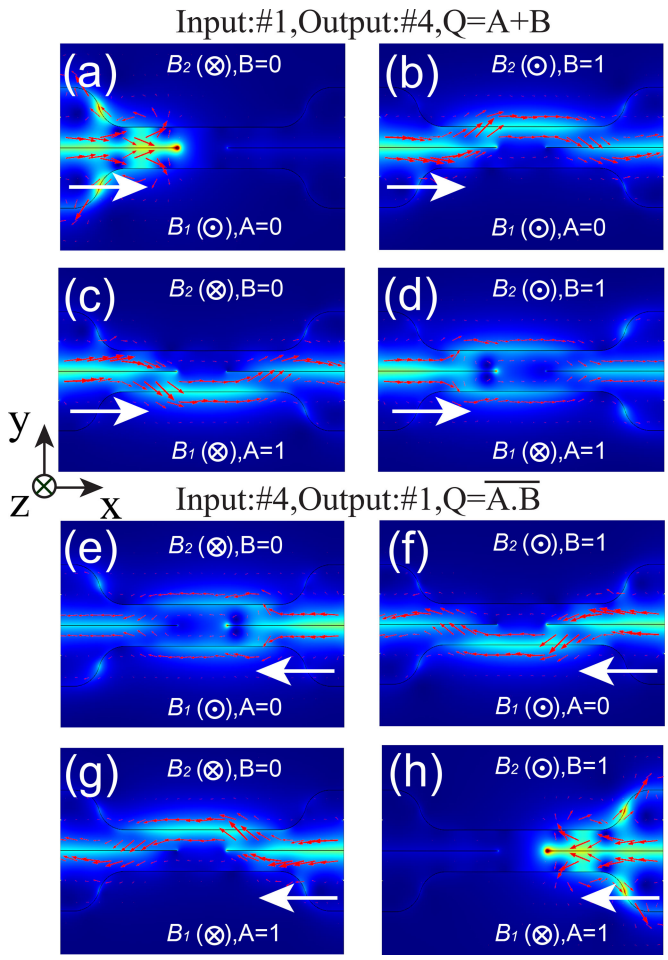

Fig. 6. The normalized $|E|$ field profiles with opposite input directions (white arrows) and applied magnetic fields. Power flow directions are illustrated with red arrow. The $L_2 = 250$ nm and $D = 60$ nm.

For the GPs input from port #4, whether the strong coupling occurs or not depends on if the wavenumbers are matched between plasmons on middle graphene layer and those on InSb substrate along x^- direction. Either a magnetic field B_1 along z^- direction (input logic A = 0) or a magnetic field B_2 along z^+ direction (input logic B = 0) ensures the output of GPs from port #1 (output logic $Q = 1$). Only when both B_1 along z^+ direction (input logic A = 1) and B_2 along z^- direction (input logic B = 1) are satisfied, the output of port #1 is low (output logic $Q = 0$). Afterwards, the plasmons would be reflected and output from port #5 and port #6 [see Fig. 6(h)]. Such mechanism can be explained via the Boolean algebra, in which the output of OR logic gate can be expressed by: $Q = \mathrm{A} + \mathrm{B}$. While if we reverse the propagation direction, each input logic would be inversed as well and the output logic should be: $Q = \overline{A}+\overline{B} = \overline{A.B}$, which is just the Boolean expression of NAND logic gate. Meanwhile, the normalized electric field profiles according to the four groups of input logics are shown in Fig. 6(e)–(h).

IV. Magnetically-Controlled AND(NOR) Logic Gates Based on Non-Reciprocal Coupling

In the Section III, we design a magnetically-controlled logic gate based on non-reciprocal coupling, which behaves as a OR

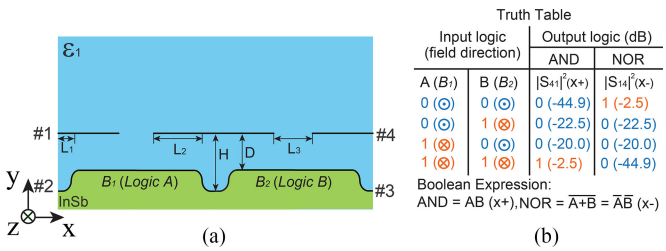

Fig. 7. The schematic of proposed AND (NOR) logic gate. The truth table is shown in (b). The wavelength is $\lambda = 9.5$ μm.

logic gate for GPs input from port #1 while as a NAND logic gate for GPs input from port #4. The inherent mechanism can be explained via Boolean algebra, which may inspire us to design another functional logic gate with similar properties. Since in Boolean algebra, the output of AND logic gate can be expressed as: $Q = A.B$. While if the two input logics are inversed respectively, the Boolean expression turns into $Q = \overline{A}.\overline{B} = \overline{A+B}$, which is just the Boolean expression of the NOR logic gate. Therefore such non-reciprocal coupling enables us to design a magnetically-controlled logic gate which behaves as AND logic gate for GPs along x^+ direction while as NOR logic gate for GPs along x^- direction.

As shown in Fig. 7(a), three top graphene layers are embedded within dielectric medium. Below them are one graphene layer deposited on InSb substrate with three trenches. The left and right substrate regions are biased with magnetic fields with same amplitude ($|B_1| = |B_2| = 3T$). The functionality of such AND (NOR) logic gate is presented through the truth table, which has been shown in the Fig. 7(b). Similar to the OR (NAND) logic gate in Fig. 5, the input logics are denoted by the directions of magnetic field B_1 and B_2, which are shown in the parenthesis of the left two columns. The value of input logic A or B is shown outside the parenthesis with the direction along z^+ direction is assumed as the high input logic. For the right two columns, the values outside the parenthesis are the output logic of such device. The transmittances through output ports are denoted as the output logic of device and the values inside parenthesis are the output energy in unit of dB.

For the GPs input from port #1, the condition of strong coupling occurs as wavenumbers of those plasmons on middle layer are matched to the ones on InSb substrates along x^+ direction. The input GPs output from port #4 if and only if both applied magnetic fields B_1 and B_2 are along z^+ direction (i.e., input logic A = B = 1). The insertion loss in such case is 2.5 dB. The direction reverse of either one of the two applied magnetic fields leads to the reflection of GPs, which afterwards output from port #2 with insertion loss larger than 20 dB. The outputs of such an AND logic gate are shown in the truth table of Fig. 7(b), in which the minimum extinction ratios as 17.5 dB can be achieved. For better presentation, we simultaneously illustrate the normalized electric field profiles according to the four groups of input logics in Fig. 8(a)–(d).

For the GPs input from port #4, the input plasmons could pass through such architecture if and only if both applied magnetic fields B_1 and B_2 are along z^- direction (i.e., input logic A = B = 0). Either the magnetic field B_1 along z^+ direction (i.e.,

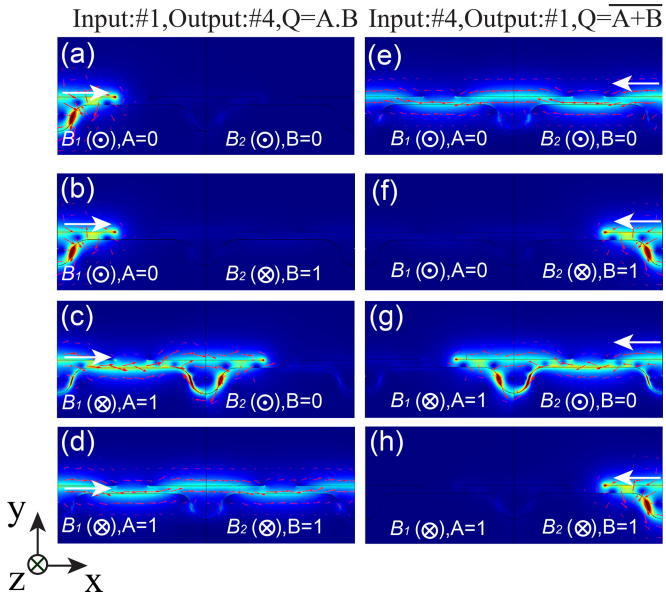

Fig. 8. The normalized $|E|$ field profiles with opposite input directions (white arrows) and applied magnetic fields. Power flow directions are illustrated with red arrow. The $L_2 = 180$ nm and $D = 40$ nm.

input logic A = 1) or the magnetic field B_2 along z^+ direction (i.e., input logic B = 1) leads to the reflection of input GPs and their output from port #3. The outputs of such an NOR logic gate are shown in the truth table of Fig. 7(b). Meanwhile, the normalized electric field profiles according to the four groups of input logics are shown in Fig. 8(e)–(h). The red arrows are power flow directions and white arrows are plasmons input directions.

Compared with the previously reported electronically- controlled GPs logic gates in which the graphene layers are individually biased and each functional logic gate needs specific biasing implement [13], the magnetically-controlled logic gates present several advantages. Firstly, all the graphene layers are chemical doped and no electronically biasing is needed. Secondly, the output logic is controlled by the direction of magnetic field instead of amplitude of voltage, reducing the implementation complexities. Finally, combined with the non-reciprocal coupling mechanism, the proposed logic gates possess special functionalities, namely the function of logic gate also depends on the input directions of GPs, which provides high complexity in the practical applications.

Via the Boolean algebra, we design in this paper OR (NAND) and NOR (AND) logic gates possessing one logic function while another when the plasmons input from opposite direction. Although the analogy of traditional XOR logic gate with only two input control signals is hard to achieve by simply cascading multiple magnetically-controlled NAND logic gates, it can be obtained by adding a π-phase difference between plasmons propagating along top and bottom graphene layers in OR logic gate structure to ensure a destructive interference at the recombination point, which has been also adopted in the electrical controlled graphene logic gates previously [13]. In this case, reversing the input plasmons direction would not affect the specific function of logic gates. Since in Boolean algebra, the XOR gate is expressed as $Q = \overline{A}.B + A.\overline{B}$, simply inversing the input logics would not change output.

V. Conclusion

In conclusion, we propose the magnetically-controlled GPs logic gates based on non-reciprocal coupling. The magnetic-optical effect based non-reciprocal coupling allows for the complete energy coupling in only one direction between two vertically placed graphene layers. The transmittance of such non-reciprocal coupling can be well explained by theoretical model based on CMT. Furthermore, such effect enables us to control the output of logic gate by reversing plasmons propagation direction. According to the Boolean algeria, we design two functional logic gates which behave as OR or AND logic gates for plasmons along x^+ direction while as NAND or NOR logic gates for plasmons along x^- direction. By choosing capable geometrical parameters, the minimum extinction ratio for OR (NAND) logic gate is 13.6 dB while for AND (NOR) logic gate is 17.5 dB. The proposed magnetically-controlled logic gates may provide new functionalities in graphene-based plasmonics devices.

References

[1] L. A. Falkovsky, "Optical properties of graphene and IV–VI semiconductors," *Phys.-Uspekhi*, vol. 51, no. 9, pp. 887–897, Mar. 2008.
[2] F. Liu, C. Qian, and Y. D. Chong, "Directional excitation of graphene surface plasmons," *Opt. Exp.*, vol. 23, no. 3, pp. 2383–2391, Jan. 2015.
[3] W. Gao, J. Shu, C. Qiu, and Q. Xu, "Excitation of plasmonic waves in graphene by guided-mode resonances," *ACS Nano*, vol. 6, no. 9, pp. 7806–7813, Sep. 2012.
[4] J. Tao, X. Yu, B. Hu, A. Dubrovkin, and Q. J. Wang, "Graphene-based tunable plasmonic Bragg reflector with a broad bandwidth," *Opt. Lett.*, vol. 39, no. 2, pp. 271–274, Jan. 2014.
[5] B. Biel, F. Triozon, X. Blase, and S. Roche, "Chemically induced mobility gaps in graphene nanoribbons: A route for upscaling device performances," *Nano Lett.*, vol. 9, no. 7, pp. 2725–2729, Jul. 2009.
[6] J. Brion, R. Wallis, A. Hartstein, and E. Burstein, "Theory of surface magnetoplasmons in semiconductors," *Physical Rev. Lett.*, vol. 28, no. 22, pp. 1455–1458, May 1972.
[7] B. Xu *et al.*, "Terahertz light deflection in doped semiconductor slit arrays," *Opt. Commun.*, vol. 308, pp. 74–77, Jul. 2013.
[8] L. Demkó *et al.*, "Enhanced infrared magneto-optical response of the non-magnetic semiconductor BiTeI driven by bulk Rashba splitting," *Physical Rev. Lett.*, vol. 109, no. 16, pp. 167401-1–167401-5, Oct. 2012.
[9] S. A. Maier, *Plasmonics: Fundamentals and Applications*. New York, NY, USA: Springer-Verlag, 2007.
[10] H. Iizuka and S. H. Fan, "Deep subwavelength plasmonic waveguide switch in double graphene layer structure," *Appl. Phys. Lett.*, vol. 103, no. 23, pp. 233107-1–233107-5, Dec. 2013.
[11] B. Wang, X. Zhang, X. Yuan, and J. Teng, "Optical coupling of surface plasmons between graphene sheets," *Appl. Phys. Lett.*, vol. 100, no. 13, pp. 131111-1–131111-4, Mar. 2012.
[12] S. Joo *et al.*, "Magnetic-field-controlled reconfigurable semiconductor logic," *Nature*, vol. 494, no. 7435, pp. 72–76, Feb. 2013.
[13] K. J. Ooi, H. S. Chu, P. Bai, and L. K. Ang, "Electro-optical graphene plasmonic logic gates," *Opt. Lett.*, vol. 39, no. 6, pp. 1629–1632, Mar. 2014.

Bofeng Zhu received the B.S. degree in electronic science and technology from Beijing Jiaotong Unversity, Beijing, China, in 2012.

He is currently working toward the Ph.D. degree in communication and information systems at the Institute of Lightwave Technology. His current research interests include the graphene plasmonics devices, graphene-based metameterials, and fiber optical communication.

Guobin Ren received the Ph.D. degree in communication and information systems from Beijing Jiaotong University, Beijing, China, in 2005.

In 2006, he joined the Network Technology Research Center, Nanyang Technological University, Singapore, as a Research Fellow. In 2011, he joined the Institute of Lightwave Technology, Key Laboratory of All Optical Network and Advanced Telecommunication Network of EMC, Beijing Jiaotong University. His research interests include optical communications, fiber optics, specialty optical fiber, and metamaterial-based devices.

Yixiao Gao received B.S. degree in physics from Beijing Jiaotong University, Beijing, China, in 2012, where he is currently working toward the Ph.D. degree in communication and information systems.

His research interests include specialty optical fiber and surface plasmons.

Beilei Wu was born in Shanxi province, China, in 1990. She received the B.S. degree from Beijing jiaotong University, Beijing, China, in 2012, where she is currently working toward the Ph.D. degree in communication and information systems at the Institute of Lightwave Technology.

Her research interest includes microwave photonics.

Chenglong Wan is currently working toward the Ph.D. degree in electrical and electronic engineering at the University of Bristol, Bristol, U.K.

He is affiliated with the Photonics Research Group, University of Bristol. His current research interest includes metamaterial for solar thermal applications

Shuisheng Jian is the Director of the Institute of Lightwave Technology, a Member of the Chinese Academy of Sciences, the Chairman of the Academic Committee of Beijing Jiaotong University, and the Director of the Institute of Light Wave.

He is a well-known Specialist in optical fiber communication, optical fiber sensing, optical fiber devices, and optical fiber network in China.